arXiv:1906.08742v1 [gr-qc] 20 Jun 2019

Rotating wormhole solutions with a complex phantom scalar field

Xiao Yan Chew,[1,*] Vladimir Dzhunushaliev,[2,3,4,1,†] Vladimir Folomeev,[2,4,1,‡] Burkhard Kleihaus,[1,§] and Jutta Kunz[1,¶]

[1] *Institut für Physik, Universität Oldenburg, Postfach 2503 D-26111 Oldenburg, Germany*
[2] *Institute of Experimental and Theoretical Physics, Al-Farabi Kazakh National University, Almaty 050040, Kazakhstan*
[3] *Department of Theoretical and Nuclear Physics, Al-Farabi Kazakh National University, Almaty 050040, Kazakhstan*
[4] *Academician J. Jeenbaev Institute of Physics of the NAS of the Kyrgyz Republic, 265 a, Chui Street, Bishkek 720071, Kyrgyz Republic*

(Dated: October 20, 2021)

We consider rotating wormhole solutions supported by a complex phantom scalar field with a quartic self-interaction, where the phantom field induces the rotation of the spacetime. The solutions are regular and asymptotically flat. A subset of solutions describing static but not spherically symmetric wormholes is also obtained.

PACS numbers: 04.20.Jb, 04.40.-b

I. INTRODUCTION

Wormholes have received much attention in recent years. Numerous investigations have been performed addressing the possible signatures of wormholes in astrophysical searches, including gravitational lensing by wormholes [1–12], shadows of wormholes [10, 13–16], or accretion disks around wormholes [17–21]. Particular emphasis has been placed on the question as to what extent wormholes might mimick black holes [10, 22–29].

As discussed by Morris and Thorne [30, 31] the presence of exotic matter allows for the construction of wormholes in General Relativity. The simplest such wormhole solutions are the Ellis wormholes, which are obtained with a real massless phantom field [32–37], i.e., a scalar field whose kinetic term has the opposite sign as compared to ordinary scalar fields. The static Ellis wormholes are known in closed form. Their rotating generalizations, however, are either known perturbatively [38, 39] or numerically [40–42].

Whereas the static Ellis wormholes can be chosen to be symmetric with respect to reflection at the throat such that both parts of the spacetime are completely alike, the presence of rotation necessarily breaks this symmetry for Ellis wormholes [38–42]. (For the discussion of rotating Ellis wormholes in Scalar-Tensor Theories see [43]). The presence of further ordinary fields, however, can allow for reflection symmetric rotating wormholes, as recently shown for the case of an ordinary complex scalar field [44]. In fact, in these configurations the rotation of the wormhole is induced by the rotation of the matter fields.

Besides a real phantom field one can, however, also consider a complex phantom field. In that case one can try to impose rotation directly on the complex phantom field, and thus obtain rotating wormhole configurations that are symmetric and do not need any additional matter fields. This is the goal of the present work.

Non-rotating wormholes based on a complex phantom field with a *Mexican hat* type potential have been considered before [45]. The $U(1)$ symmetry of the theory leads to a conserved current associated with a conserved charge, the particle number. As in boson stars [46–49] the phantom field of the wormholes possesses a harmonic time-dependence, while their metric is static and spherically symmetric. However, there exist also wormhole solutions, where the time-dependence of the phantom field vanishes together with the particle number. For these solutions the complex phantom field reduces to a real valued field.

Here we impose rotation on the complex phantom field in the same way that rotation is imposed for an ordinary complex scalar field in the construction of boson stars [50–56] or of wormholes immersed in rotating bosonic matter [44, 57]. Thus the ansatz for the complex phantom field has an explicit dependence on the azimuthal angle featuring

*Electronic address: xiao.yan.chew@uni-oldenburg.de
†Electronic address: v.dzhunushaliev@gmail.com
‡Electronic address: vfolomeev@mail.ru
§Electronic address: b.kleihaus@uni-oldenburg.de
¶Electronic address: jutta.kunz@uni-oldenburg.de

an integer n for spatial single-valuedness of the solutions, as in the well-known case of the spherical harmonics. The rotating solutions then do not only possess a mass and a particle number, but they also carry an angular momentum proportional to the particle number with proportionality constant n, a relation well-known from boson stars.

The paper is organized as follows. In section II we present the action, Ansätze, field equations and boundary conditions, and we define various physical quantities. In section III we present the solutions. We first briefly recall the non-rotating case, and then discuss the properties of the rotating solutions, where we analyze the global charges and the wormhole geometries. We give our conclusions in section IV.

II. THEORETICAL SETTING

In this section we present the action, the Ansätze for the metric and the phantom field, the resulting field equations and the boundary conditions. Subsequently we define the global charges and the geometrical properties of the wormholes.

A. Action

The action consists of the Einstein-Hilbert action and the action for a complex phantom field

$$S = \int \left[\frac{1}{2\kappa}\mathcal{R} + \mathcal{L}_{\rm ph}\right] \sqrt{-g}\; d^4x \; . \tag{1}$$

Here $\mathcal{R}$ is the curvature scalar, $\kappa = 8\pi G$ is the coupling constant, g denotes the determinant of the metric, and $\mathcal{L}_{\rm ph}$ represents the Lagangian of the complex phantom field Φ

$$\mathcal{L}_{\rm ph} = \frac{1}{2} g^{\mu\nu} \left(\partial_\mu \Phi^* \partial_\nu \Phi + \partial_\nu \Phi^* \partial_\mu \Phi\right) - V(|\Phi|^2) \; , \tag{2}$$

where the asterisk represents complex conjugation and the potential V

$$V(|\Phi|^2) = -m_{\rm ph}^2 |\Phi|^2 + \Lambda |\Phi|^4 \tag{3}$$

consists of a mass term with boson mass parameter $m_{\rm ph}$ and a quartic self-interaction term with coupling parameter Λ. For the discussion of the potential see [45].

Variation of the action with respect to the metric and the phantom field lead to the Einstein equations

$$G_{\mu\nu} = \mathcal{R}_{\mu\nu} - \frac{1}{2} g_{\mu\nu} \mathcal{R} = \kappa T_{\mu\nu} \tag{4}$$

with stress-energy tensor

$$T_{\mu\nu} = g_{\mu\nu} \mathcal{L}_{\rm ph} - 2 \frac{\partial \mathcal{L}_{\rm ph}}{\partial g^{\mu\nu}} \; , \tag{5}$$

and to the phantom field equation

$$\nabla^\mu \nabla_\mu \Phi = m_{\rm ph}^2 \Phi - 2\Lambda |\Phi|^2 \Phi. \tag{6}$$

It is convenient to introduce dimensionless quantities

$$\hat{\Phi} = \sqrt{\kappa}\Phi \; , \quad \hat{\eta} = \frac{1}{\lambda}\eta \; , \tag{7}$$

where η is the radial coordinate (see Eq. (10)). Consequently,

$$\hat{G}_{\mu\nu} = \hat{T}_{\mu\nu} \; , \tag{8}$$

where the potential $-\hat{m}_{\rm ph}^2 |\hat{\Phi}|^2 + \hat{\Lambda} |\hat{\Phi}|^4$ on the right hand side contains the dimensionless parameters

$$\hat{m}_{\rm ph} = \left(\frac{m_{\rm ph}}{m_{\rm P}}\right) \left(\frac{M_0}{m_{\rm P}}\right) \; , \quad \hat{\Lambda} = \left(\frac{M_0}{m_{\rm P}}\right)^2 \frac{1}{8\pi} \Lambda \; . \tag{9}$$

Here $m_{\rm P}$ denotes the Planck mass, and the mass scale M_0 is related to the length scale by $M_0 = \lambda/G$. We will omit the hats in the following for reasons of notational simplicity.

B. Ansätze

To incorporate the non-trivial topology we employ as line element for the metric

$$ds^2 = -e^f dt^2 + e^{q-f}\left[e^b(d\eta^2 + h d\theta^2) + h\sin^2\theta(d\varphi - \omega dt)^2\right] \ , \tag{10}$$

where the functions f, q, b and ω depend on the radial coordinate η and the polar angle θ, and the auxiliary function $h = \eta^2 + \eta_0^2$ contains the throat parameter η_0. The radial coordinate η covers the interval $-\infty < \eta < \infty$, where both limits $\eta \to \pm\infty$ represent asymptotically flat regions.

For the complex phantom field we adopt the Ansatz

$$\Phi(t,\eta,\theta,\varphi) = \phi(\eta,\theta)\ e^{i\omega_s t + in\varphi} \tag{11}$$

with the real function $\phi(\eta,\theta)$, the real boson frequency ω_s and the integer winding number n. This Ansatz agrees with the one employed for rotating Q-balls and boson stars [50–56] and for wormholes immersed in rotating bosonic matter [44, 57]. Non-rotating, spherically symmetric solutions can be obtained with the Ansatz Eqs. (10) and (11) for $n = 0$ with $b = 0$, $\omega = 0$, and the remaining functions depending on η only.

C. Einstein and Matter Field Equations

By substituting the Ansätze (10) and (11) into the set of Einstein equations $E_\mu^\nu = G_\mu^\nu - T_\mu^\nu = 0$, we find the following set of equations

$$f_{,\eta\eta} + \frac{f_{,\theta\theta}}{h} + f_{,\eta}\frac{hq_{,\eta} + 4\eta}{2h} + f_{,\theta}\frac{2\cot\theta + q_{,\theta}}{2h} - e^{q-2f}\sin^2\theta\left(h\omega_{,\eta}^2 + \omega_{,\theta}^2\right) = -2\left[2(n\omega+\omega_s)^2\phi^2 + V(\phi^2)e^f\right]e^{b+q-2f} \ , \tag{12}$$

$$q_{,\eta\eta} + \frac{q_{,\theta\theta}}{h} + \frac{q_{,\eta}^2}{2} + \frac{3\eta q_{,\eta}}{h} + \frac{q_{,\theta}^2}{2h} + \frac{2q_{,\theta}\cot\theta}{h} = -4\left(e^{q-2f}h\left[(n\omega+\omega_s)^2\phi^2 + V(\phi^2)e^f\right]\sin^2\theta - n^2\phi^2\right)\frac{e^b}{h\sin^2\theta} \ , \tag{13}$$

$$\begin{aligned} & b_{,\eta\eta} + \frac{b_{,\theta\theta}}{h} + b_{,\eta}\frac{\eta}{h} \\ & + \frac{1}{2}\left[f_{,\eta}^2 + \frac{f_{,\theta}^2}{h} - q_{,\eta}^2 - \frac{q_{,\theta}^2}{h} - \frac{4}{h}\left(\cot\theta q_{,\theta} + \eta q_{,\eta}\right) + \frac{4}{h}\left(1 - \frac{\eta^2}{h}\right) - 3e^{q-2f}h\left(\omega_{,\eta}^2 + \frac{\omega_{,\theta}^2}{h}\right)\sin^2\theta\right] \\ = \ & 2\left(\phi_{,\eta}^2 + \frac{\phi_{,\theta}^2}{h}\right) + 2\left(e^{q-2f}h\left[(n\omega+\omega_s)^2\phi^2 + V(\phi^2)e^f\right]\sin^2\theta - 3n^2\phi^2\right)\frac{e^b}{h\sin^2\theta} \ , \end{aligned} \tag{14}$$

$$\omega_{,\eta\eta} + \frac{\omega_{,\theta\theta}}{h} + \frac{\omega_{,\eta}}{2}\left(3q_{,\eta} - 4f_{,\eta} + \frac{8\eta}{h}\right) + \frac{\omega_{,\theta}}{2h}\left(3q_{,\theta} - 4f_{,\theta} + 6\cot\theta\right) = -4n(n\omega+\omega_s)\phi^2\frac{e^b}{h\sin^2\theta} \ , \tag{15}$$

resulting from $E_t^t = 0$, $E_\eta^\eta + E_\theta^\theta = 0$, $E_\varphi^\varphi = 0$ and $E_\varphi^t = 0$, respectively. From $d := E_\eta^\eta - E_\theta^\theta$ we find in addition the condition

$$\begin{aligned} d = 0 \ = \ & q_{,\eta\eta} - \frac{1}{h}q_{,\theta\theta} - \left(\omega_{,\eta}^2 - \frac{1}{h}\omega_{,\theta}^2\right)h\sin^2\theta e^{-2f+q} - \frac{1}{2}\left(q_{,\eta}^2 - \frac{1}{h}q_{,\theta}^2\right) + \left(f_{,\eta}^2 - \frac{1}{h}f_{,\theta}^2\right) \\ & - \frac{1}{h}\left(q_{,\eta}\left(hb_{,\eta} + \eta\right) - q_{,\theta}b_{,\theta}\right) - \frac{2}{h^2\sin\theta}\left[\left(\eta\sin\theta b_{,\eta} - \cos\theta b_{,\theta}\right)h - 2\eta_0^2\sin\theta\right] \\ & - 4\left(\phi_{,\eta}^2 - \frac{1}{h}\phi_{,\theta}^2\right) \ . \end{aligned} \tag{16}$$

to which we refer to as constraint. The field equation for the phantom field function $\phi(\eta,\theta)$ is obtained from Eq. (6),

$$\phi_{,\eta\eta} + \frac{\phi_{,\theta\theta}}{h} + \frac{\phi_{,\eta}}{2}\left(q_{,\eta} + 4\frac{\eta}{h}\right) + \frac{\phi_{,\theta}}{2h}\left(q_{,\theta} + 2\cot\theta\right) + \left(e^{q-2f}h\left[(n\omega+\omega_s)^2 + \frac{dV(\phi^2)}{d\phi^2}e^f\right]\sin^2\theta - n^2\right)\phi\frac{e^b}{h\sin^2\theta} = 0 \ . \tag{17}$$

Inspection of the system of equations shows that it is symmetric with respect to reflection of the radial coordinate, $\eta \to -\eta$. Consequently reflection symmetric solutions will exist, although non-symmetric solutions might exist as well. Since in this study we will consider only reflection symmetric solutions, it is sufficient to restrict the computations to the interval $0 \le \eta < \infty$, where $\eta = 0$ corresponds to the wormhole throat.

We note that η_0 is not a free parameter, when ω_s and Λ are freely varied. Instead, for any value of ω_s and Λ, η_0 has to be chosen such that the constraint Eq. (16) is satisfied.

D. Boundary Conditions

Let us now specify the boundary conditions employed to solve the above set of five coupled partial differential equations (PDEs) of second order. In particular, we need to impose conditions for each function at the boundaries of the domain of integration. These consist of the throat at $\eta = 0$, the axis of rotation $\theta = 0$, the equatorial plane $\theta = \pi/2$, and the asymptotic region $\eta \to \infty$.

Guided by symmetry arguments, we now specify our detailed choice of boundary conditions. Asking for reflection symmetry means that the normal derivatives of all functions have to vanish at the throat,

$$\partial_\eta f(\eta,\theta)|_{\eta=0} = \partial_\eta q(\eta,\theta)|_{\eta=0} = \partial_\eta b(\eta,\theta)|_{\eta=0} = \partial_\eta \omega(\eta,\theta)|_{\eta=0} = \partial_\eta \phi(\eta,\theta)|_{\eta=0} = 0 \ . \tag{18}$$

We demand that the metric should be asymptotically flat and the phantom field should vanish asymptotically

$$f(\eta,\theta)|_{\eta\to\infty} = q(\eta,\theta)|_{\eta\to\infty} = b(\eta,\theta)|_{\eta\to\infty} = \omega(\eta,\theta)|_{\eta\to\infty} = \phi(\eta,\theta)|_{\eta\to\infty} = 0 \ . \tag{19}$$

Reflection symmetry with respect to the equatorial plane leads to the conditions

$$\partial_\theta f(\eta,\theta)|_{\theta=\frac{\pi}{2}} = \partial_\theta q(\eta,\theta)|_{\theta=\frac{\pi}{2}} = \partial_\theta b(\eta,\theta)|_{\theta=\frac{\pi}{2}} = \partial_\theta \omega(\eta,\theta)|_{\theta=\frac{\pi}{2}} = \partial_\theta \phi(\eta,\theta)|_{\theta=\frac{\pi}{2}} = 0 \ . \tag{20}$$

Regularity along the rotation axis requires

$$\partial_\theta f(\eta,\theta)|_{\theta=0} = \partial_\theta q(\eta,\theta)|_{\theta=0} = \partial_\theta \omega(\eta,\theta)|_{\theta=0} = 0 \ , \quad b(\eta,\theta)|_{\theta=0} = 0 \ , \quad \phi(\eta,\theta)|_{\theta=0} = 0 \ . \tag{21}$$

For the non-rotating solutions the last boundary condition has to be replaced by $\partial_\theta \phi(\eta,\theta)|_{\theta=0} = 0$.

E. Mass, angular momentum and particle number

Let us now address the global charges of the solutions. The (dimensionless) mass M and the (dimensionless) angular momentum J can be obtained from the corresponding Komar integrals and read off from the asymptotic behaviour of the metric functions

$$f \longrightarrow -\frac{2M}{\eta} \ , \quad \omega \longrightarrow \frac{2J}{\eta^3} \quad \text{as } \eta \to \infty \ . \tag{22}$$

The Komar integrals can also be transformed with the help of the Einstein equations to yield

$$M = \int (2T^t_t - T^\mu_\mu)\sqrt{-g} dr d\theta d\varphi \ , \tag{23}$$

and

$$J = -\int T^t_\varphi \sqrt{-g} dr d\theta d\varphi \ . \tag{24}$$

The particle number Q is a Noether charge, associated with the conserved $U(1)$ current,

$$Q = \int_\Sigma j_\mu n^\mu dV \ , \tag{25}$$

where the integrand corresponds to $-j^t\sqrt{-g}$. As noted by Schunck and Mielke [50, 51] in the case of boson stars, $T^t_\varphi = nj^t$. By comparing Eqs. (25) and (24) one then finds the relation between angular momentum and particle number [50–56]

$$J = nQ \ . \tag{26}$$

This relation is also known to hold for symmetric wormholes immersed in rotating bosonic matter [44], and it also holds for the symmetric wormholes with a complex phantom field studied here.

F. Wormhole throat

The most important geometrical property of the solutions is their throat. To analyze the throat structure we consider the circumferential radius $R_e(\eta)$ in the equatorial plane,

$$R_e(\eta) = \sqrt{h}\, e^{\frac{q-f}{2}}\Big|_{\theta=\pi/2} \ . \tag{27}$$

Clearly for large η the circumferential radius $R_e(\eta)$ diverges. However, for $\eta \to 0$ the circumferential radius reaches a minimum. The minimal surface at $\eta = 0$ therefore corresponds to the throat of the wormhole solution.

In principle, more than one minimum could exist, and in between the minima there might arise local maxima. In that case the spacetime would have multiple throats with equators in between. At $\eta = 0$ there will always either be a throat or an equator, when the solutions possess reflection symmetry.

G. Ergosurface and static orbits

The wormhole spacetimes could also feature an ergosurface,

$$g_{tt}(\eta, \theta) = 0 \ . \tag{28}$$

The condition $g_{tt} > 0$ then defines the ergoregion, whose boundary is the ergosurface.

In [58] is was shown that in stationary rotating spacetimes static orbits in the equatorial plane may exist. On this kind of orbit a particle stays at rest relative to an observer in the asymptotic region when it was at rest initially. The necessary and sufficient condition for a static orbit is that g_{tt} possesses a local maximum (stable) or a local minimum (unstable) in some region where $g_{tt} < 0$. It was demonstrated in [58] that static orbits exist for rotating boson stars and wormholes immersed in rotating matter. For symmetric wormhole solutions considered in this work g_{tt} always is extremal at the throat. Hence a static orbit always resides at the throat.

III. RESULTS

Let us now analyze the properties of the wormhole solutions based on a complex phantom field. We will first recall the non-rotating case, and subsequently we will discuss the rotating case. The wormhole solutions depend on three continuous parameters, represented by the boson mass parameter $m_{\rm ph}$, the boson frequency ω_s, and the quartic self-interaction strength Λ, and in addition on the integer winding number n, which must be non-zero in the case of rotation.

We note that the set of coupled Einstein and phantom field equations are invariant under a scaling transformation, i.e.,

$$\eta \to \lambda\eta \ , \quad \eta_0 \to \lambda\eta_0 \ , \quad \omega \to \frac{1}{\lambda}\omega \ , \quad \omega_s \to \frac{1}{\lambda}\omega_s \ , \quad m_{\rm ph} \to \frac{1}{\lambda}m_{\rm ph} \ , \quad \Lambda \to \frac{1}{\lambda^2}\Lambda \ . \tag{29}$$

To break this scaling invariance we choose for the boson mass parameter the value $m_{\rm ph} = 1$. The remaining free parameters are then the boson frequency ω_s, the coupling constant Λ, and the winding number n.

A. Non-rotating solutions

Let us start with the non-rotating wormhole solutions, which are obtained for vanishing winding number $n = 0$. The Ansatz and the field equations then simplify considerably, and a system of non-linear coupled ODEs is obtained. The properties of the non-rotating wormhole solutions have been investigated in [45]. Here we will summerize them briefly in order to be able to compare with the rotating case.

Non-rotating solutions appear to exist for all values of the coupling strength $\Lambda > 0$, and in the full interval of the boson frequency $0 \leq \omega_s \leq 1$. In Fig.1 we show the mass M, particle number Q, circumferential radius R_e and throat parameter η_0 as a function of the coupling strength Λ for several values of ω_s. For the limiting cases $\omega_s = 0$ and $\omega_s = 1$ the mass, particle number and throat radius assume finite values (except for $Q = 0$ when $\omega_s = 0$). This is in contrast to solutions with an ordinary complex scalar field describing boson stars or wormholes immersed inside bosonic matter. We emphasize that the solutions become static when $\omega_s = 0$, since the time-dependence of the phantom field then disappears.

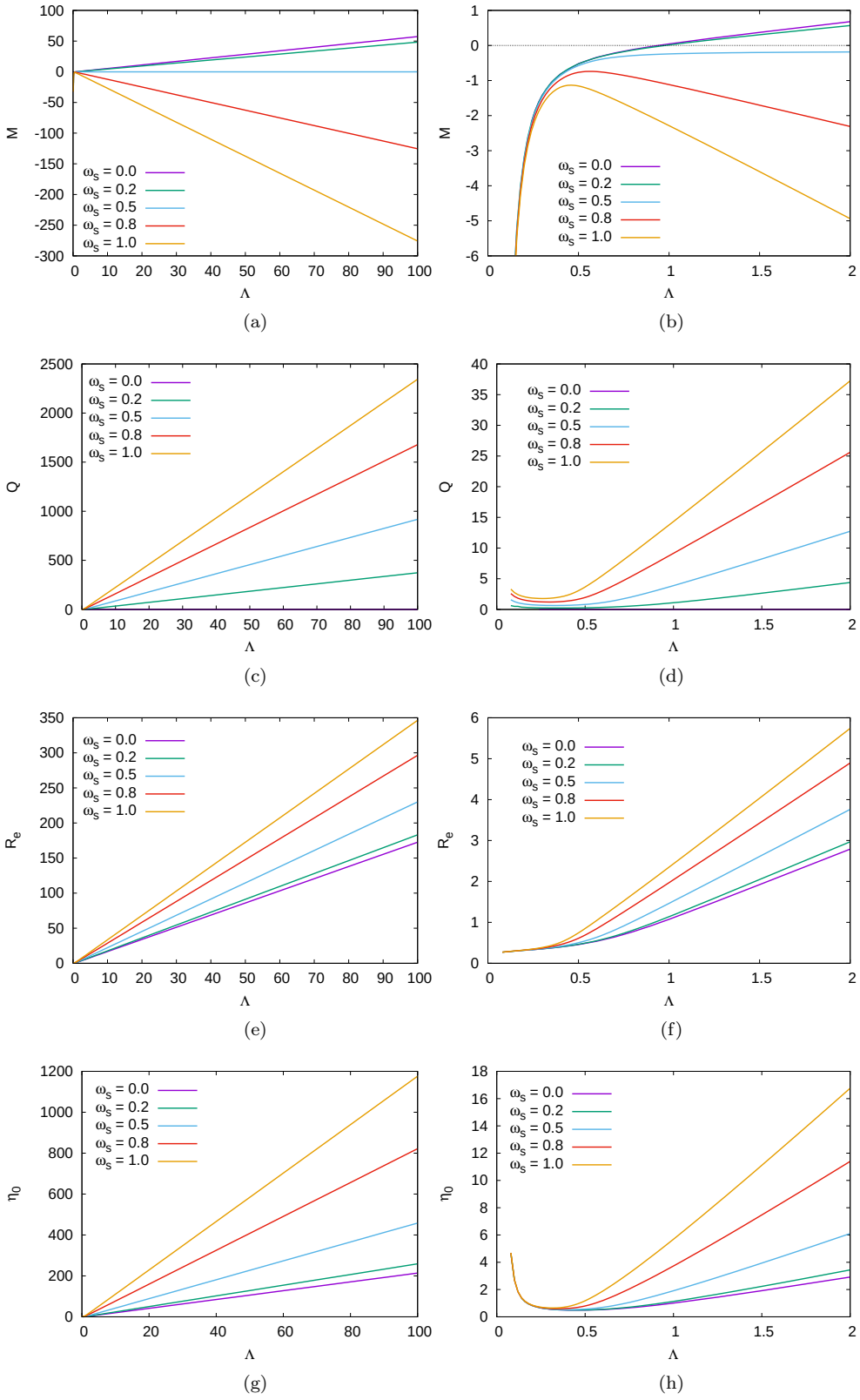


Figure 1: Properties of non-rotating wormhole solutions ($n = 0$) versus the coupling strength Λ ($0.08 \leq \Lambda \leq 100$) for several values of the boson frequency ω_s: (a) mass M; (b) zoom of (a); (c) particle nummber Q; (d) zoom of (c); (e) circumferential radius R_e; (f) zoom of (e); (g) throat parameter η_0; (h) zoom of (g);

In the limit $\Lambda \to \infty$ the particle number increases linearly with Λ. The mass increases (decreases) linearly for $\omega_s > 0.5$ ($\omega_s < 0.5$) and assumes a finite value for $\omega_s = 0.5$. The throat radius increases linearly with Λ. For small values of Λ the particle number possesses a minimum at some $\Lambda_{\rm min}$ (as long as $\omega_s \neq 0$) and increases with decreasing Λ for $\Lambda < \Lambda_{\rm min}$. The mass possesses a maximum only if $\omega_s > 0.5$. The throat radius increases with increasing Λ for large values of Λ. For small values of Λ, the throat radius tends to some finite value $R_e^{(0)}$ where $R_e^{(0)}$ is independent of ω_s. Like the radius, the throat parameter η_0 increases linearly with increasing Λ for large values of Λ and is independent of ω_s when Λ becomes small. However, in this case η_0 increases as Λ decreases.

B. Rotating solutions

We now turn to the rotating wormhole solutions. We note that in all the rotating wormhole solutions considered here it is the rotation of the phantom field which induces the rotation of the spacetime. This is very much in contrast to the rotating Ellis wormholes, where the rotation is imposed via the (asymmetric) boundary conditions [40, 41].

1. Numerical scheme

We have constructed a large number of wormhole solutions with winding number $n = 1$ numerically, covering the boson frequency interval $0 \leq \omega_s \leq 1$, and the interval for the self-interaction strength $0.7 \leq \Lambda < 2.0$. For values of Λ outside this interval the numerical errors have increased too much, to consider the solutions any longer as being fully reliable.

To solve the system of coupled partial differential equations we have employed the routine FIDISOL/CADSOL [59], which is a finite difference solver based on a Newton-Raphson scheme. We have introduced a compactified coordinate $x = \arctan(\eta)$, to obtain a finite coordinate patch. Then we have chosen a non-equidistant grid with typically 130×50 grid points in radial (x) and angular (θ) direction.

For given values of ω_s and Λ we have then adjusted the parameter η_0 such that the constraint Eq. (16) vanishes (to a given accuracy). In particular, we have introduced the L_2 norm of the constraint

$$D(\eta_0) = \sqrt{\sum_{i,j} d^2(x_i, \theta_j)} \ , \tag{30}$$

where the sum is over all inner gridpoints, and have determined the minimum of D with respect to η_0. Typical values of D at the minimum have been in the range 10^{-4}-10^{-3}, which is comparable with the L_2 norm of the solutions of the PDEs.

2. Solutions

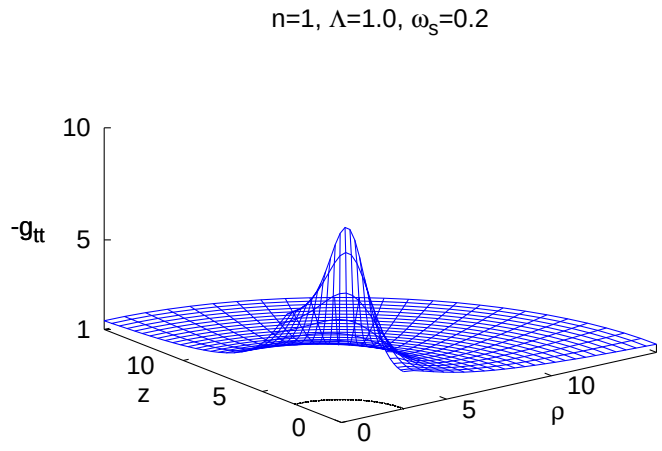
We begin our discussion by exhibiting in Fig. 2 the metric and the phantom field of a typical solution, where we have chosen the parameters $n = 1$, $\Lambda = 1$ and $\omega_{\rm s} = 0.2$. The coordinates employed in the figure are cylindrical coordinates based on an isotropic radial coordinate

$$\rho = r \sin\theta \ , \quad z = r\cos\theta \ , \quad \eta = r_0 \left(\frac{r}{r_0} - \frac{r_0}{r} \right) \ , \quad r_0 = \frac{\eta_0}{2} \ . \tag{31}$$

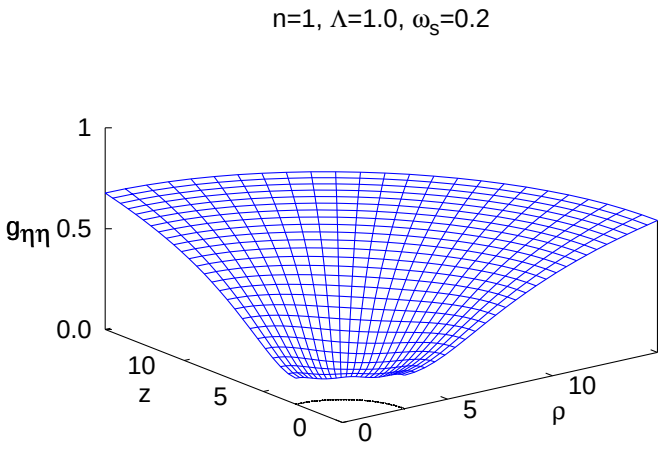
The figure shows the metric component $-g_{tt}$, the metric component $g_{\eta\eta}$, the metric component $-g_{t\varphi}$, the phantom field function ϕ. Also shown are the angular momentum density T^t_φ, and the Komar mass density $2T^t_t - T^\mu_\mu$, appearing in the Komar integrals Eqs. (24), resp. (23).

The metric functions g_{tt} and $g_{\eta\eta}$ differ most pronouncedly from their asymptotic values at the throat. Here it comes as a surprise that the maximal value of $|g_{tt}|$ does not arise at the throat in the equatorial plane. Therefore the maximum is attained on two rings on the throat, one in the upper hemisphere and one in the lower hemisphere associated with angles θ_m and $\pi - \theta_m$, respectively. The metric function $-g_{t\varphi}$ exhibits a ring of saddle points on the throat in the equatorial plane and maxima located also roughly at θ_m and $\pi - \theta_m$.

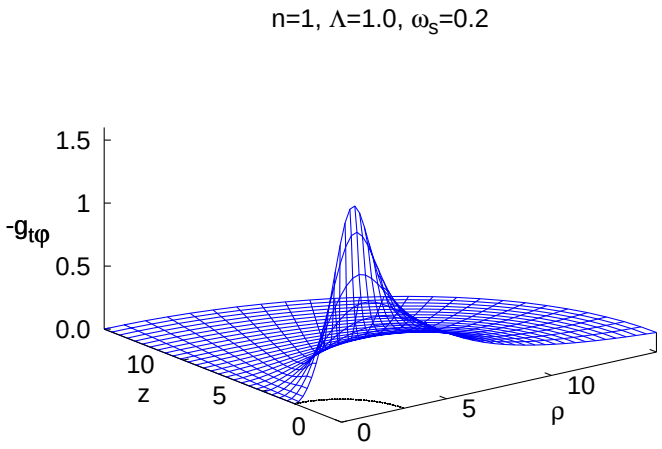
Like g_{tt} and $g_{\eta\eta}$, the phantom field function assumes its largest deviations from its vacuum value at the throat, and again the angles θ_m and $\pi - \theta_m$ indicate the rings of maxima. Therefore the rings of maxima of the angular momentum density and the Komar mass density found in the vicinity of these angles are to be expected.



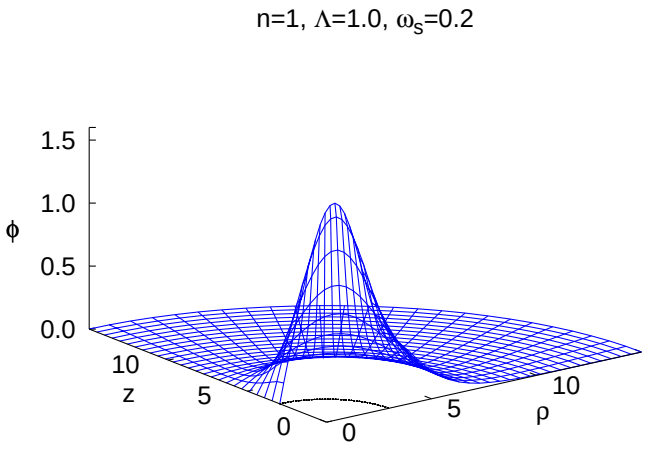
(a)



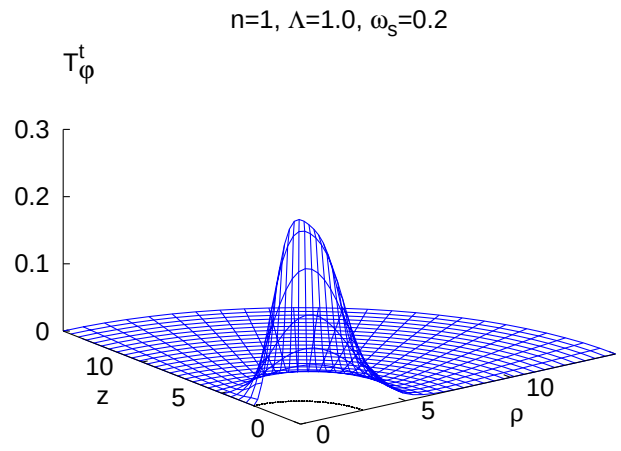
(b)



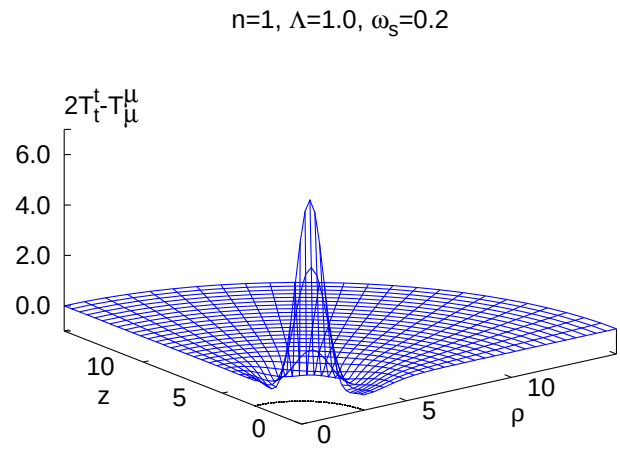
(c)



(d)

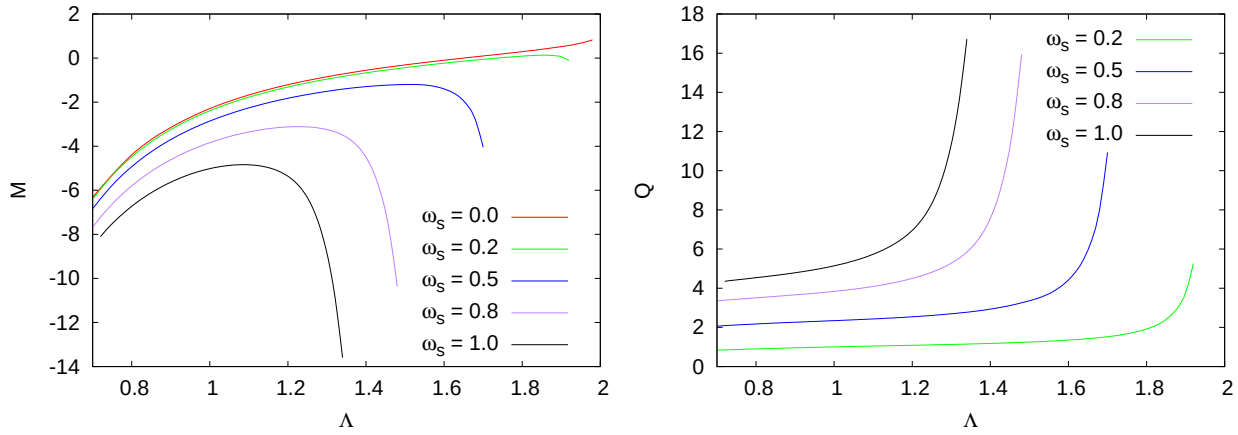


(e)



(f)

Figure 2: Rotating wormhole solution ($n = 1$, $\Lambda = 1$, $\omega_s = 0.2$): (a) metric component $-g_{tt}$; (b) metric component $g_{\eta\eta}$; (c) metric component $-g_{t\varphi}$; (d) phantom field function ϕ; (e) angular momentum density T^t_φ; (f) Komar mass density $2T^t_t - T^\mu_\mu$ in cylindrical coordinates based on an isotropic radial coordinate. The circle in the ρz-plane indicates the location of the throat.



(a) (b)

Figure 3: Global charges of rotating solutions ($n = 1$): (a) mass M versus coupling strength Λ for several values of the boson frequency ω_s; (b) same as (a) for the particle number Q.

Thus the picture we find for the metric, the phantom field and the stress energy tensor differs fundamentally from the one encountered in boson stars or wormholes immersed in ordinary rotating bosonic matter. There the matter is concentrated in a torus centered in the equatorial plane. Here the phantom matter is concentrated in two tori, located symmetrically with respect to the equatorial plane. In particular, we here find two tori for a complex field, that is symmetric with respect to reflection at $\theta = \pi/2$. Recall that double tori configurations arise for boson stars only when the complex field is antisymmetric with respect to reflection at $\theta = \pi/2$, i.e., for negative parity configurations [56].

Having noted this fundamental difference in the configurations obtained with an ordinary complex scalar field and a complex phantom field, let us address the dependence on the parameters. In fact, we observe that this fundamental difference remains, as ω_s and Λ are varied, and only the value of θ_m shifts.

Another fundamental difference to the known boson stars and wormholes immersed in ordinary rotating bosonic matter is the presence of $\omega_s = 0$ solutions. These solutions are perfectly regular, and they represent static deformed wormholes. The deformation is induced by the φ-dependence of the phantom field, since $n \neq 0$.

Concerning the presence of ergoregions, where $g_{tt} > 0$, we note that no ergoregions have emerged for the solutions we have studied so far. Also this is in constrast to boson stars and wormholes immersed in ordinary rotating bosonic matter, since those solutions are known to feature ergoregions for (sufficiently) fast rotation [44, 56, 57].

3. Global charges

Let us now turn to the global charges of the rotating wormhole solutions and their dependence on the parameters. In Fig.3 we show the mass M and the particle number Q versus the coupling strength Λ for several values of the boson frequency ω_s, including the limits $\omega_s = 0.0$ and 1.0. Recall that here the angular momentum J agrees with the particle number since $n = 1$.

We note that for $\omega_s = 0$ static solutions arise, which carry neither particle number nor angular momentum, but possess the highest mass for a given value of the coupling strength. For $\omega_s = 0$ the mass increases with increasing Λ, in the range of Λ considered.

For finite values of ω_s, the solutions rotate and possess a finite angular momentum. Whereas for the smaller values of Λ the mass first increases and then decreases, the angular momentum always increases with Λ up to a certain point, where the numerical accuracy deteriorates, and we do not depict the solutions any longer in the figure.

When the solutions are still sufficiently accurate, we note that the larger ω_s the smaller the mass for a given Λ. At the same time, the larger ω_s the earlier the rapid decrease of the mass sets in, and the earlier numerical accuracy is lost. Note that the rapid decrease of the mass goes along with a rapid increase of the particle number and angular momentum.

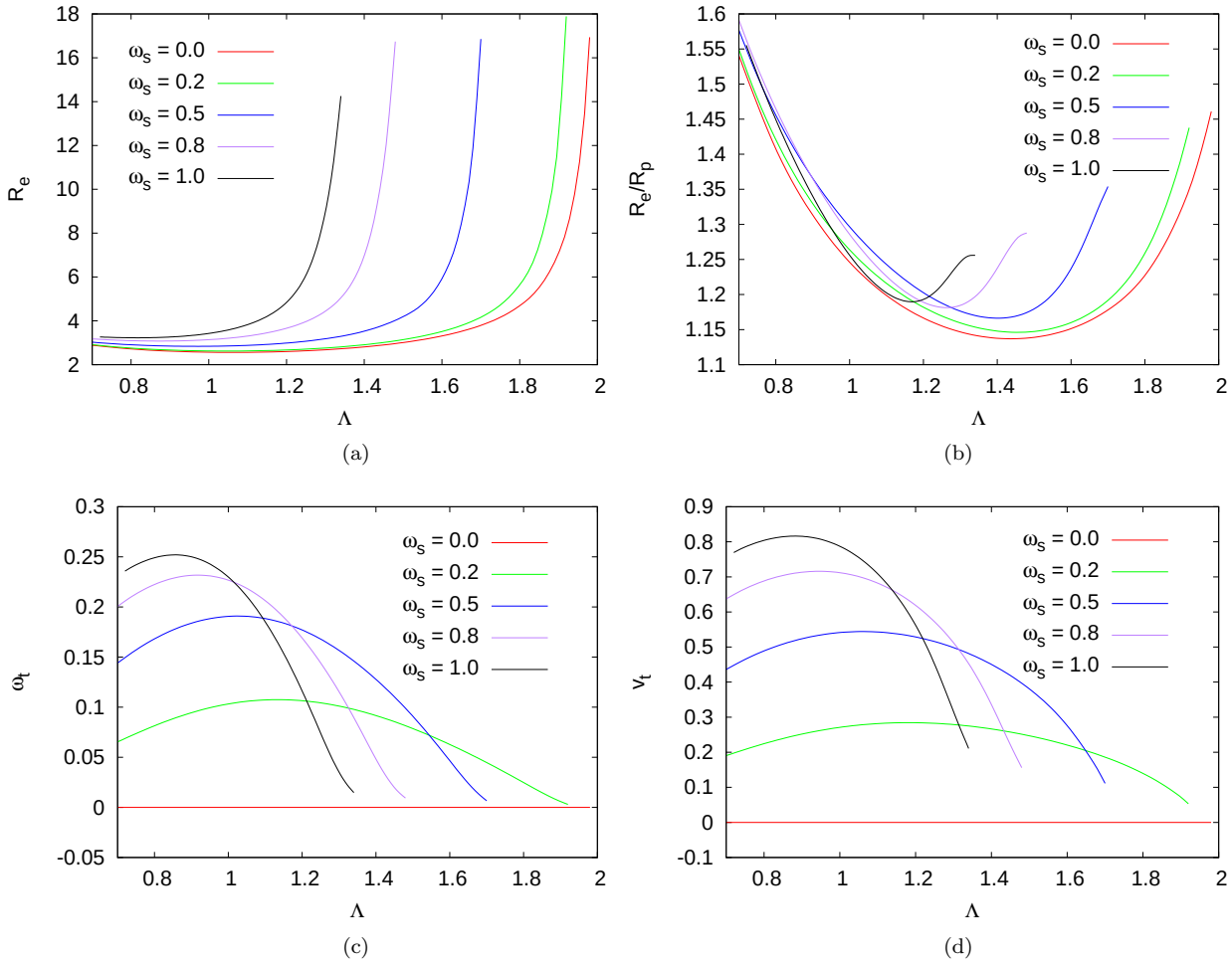


Figure 4: Geometric properties of solutions with $n = 1$ versus the coupling strength Λ for several values of the boson frequency ω_s: (a) the circumferential radius $R_{\rm e}$ of the throat in the equatorial plane; (b) the ratio of circumferential equatorial and polar radii $R_{\rm e}/R_{\rm p}$; (c) the rotational frequency $\omega_{\rm t}$ of the throat in the equatorial plane; (d) the rotational velocity $v_{\rm t}$ of the throat in the equatorial plane.

4. Geometrical properties

Let us next address the geometrical properties of the rotating solutions, focusing mostly on the equatorial plane. We present in Fig.4 the dependence on the coupling strength Λ for several physically interesting quantities: the circumferential radius $R_{\rm e}$ (a), the ratio of the circumferential equatorial and polar radii $R_{\rm e}/R_{\rm p}$ (b), the rotational frequency of the throat $\omega_{\rm t}$ in the equatorial plane (c), and the rotational velocity of the throat $v_{\rm t}$ in the equatorial plane (d), for fixed values of the boson frequency ω_s.

For a fixed boson frequency, the circumferential radius in the equatorial plane first changes slowly for the smaller values of Λ, but then exhibits a strong growth in analogy to the strong growth of the angular momentum and the strong decrease of the mass. Likewise, for a given Λ, the circumferential radius is the larger, the larger the boson frequency. Note that wormholes with multiple throats and equators have not been found in the parameter space considered.

The ratio of the polar and equatorial circumferential radii is expected to give some insight into the deformation of the throat, since for a spherical wormhole throat the ratio would be unity. Here the figure shows that this ratio starts from a large deformation at the smallest Λ considered, where it does not vary much with the boson frequency. Then the deformation decreases, reaches a minimum and increases again with increasing Λ.

The rotational frequency of the throat in the equatorial plance vanishes for $\omega_s = 0$, and its maximum increases with increasing ω_s, shifting to smaller values of Λ. When the throat rapidly increases its size with increasing Λ the rotational frequency of the throat in the equatorial plane tends towards zero. The rotational velocity of the throat in the equatorial plane follows this behavior to some extent, since it is defined by $v_t = \omega_t R_{\rm e}$.

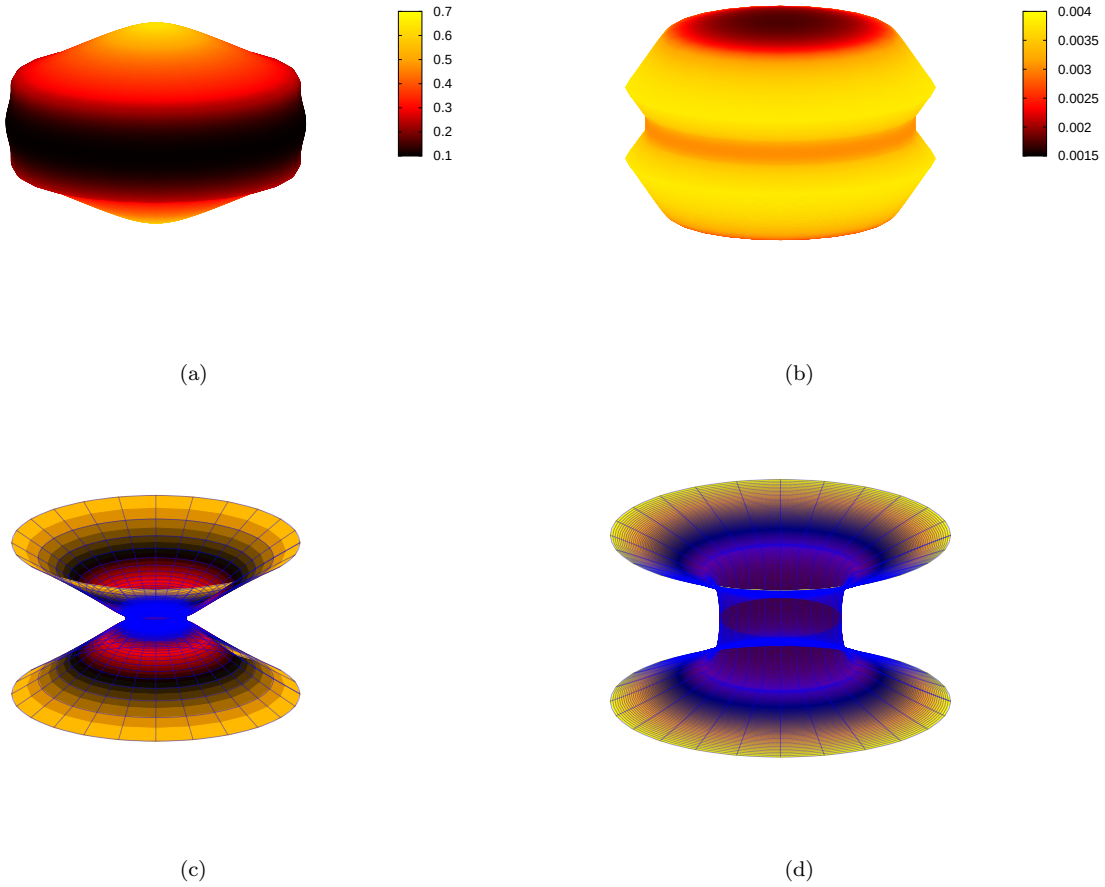


Figure 5: Rotating solutions ($n = 1$): (a) angular frequency on the embedded throat ($\omega_s = 0.2$, $\Lambda = 1$); (b) same as (a) for $\Lambda = 1.92$; (c) embedding diagram of the throat in the equatorial plane ($\omega_s = 0.2$, $\Lambda = 1$); (d) same as (c) for $\Lambda = 1.92$.

The figure nicely demonstrates that the rotation of the phantom field indeed induces a rotation of the throat and consequently a rotation of the full spacetime. However, this rotation is not uniform on the throat but depends on the polar angle. We exhibit in Fig. 5 the rotational frequency on the embedded throat for two solutions ($n = 1$, $\omega_s = 0.2$, $\Lambda = 1$ and $\Lambda = 1.92$). We note that the embedded throat deviates strongly from a sphere. Moreover, the embedding is partly pseudo-euclidean.

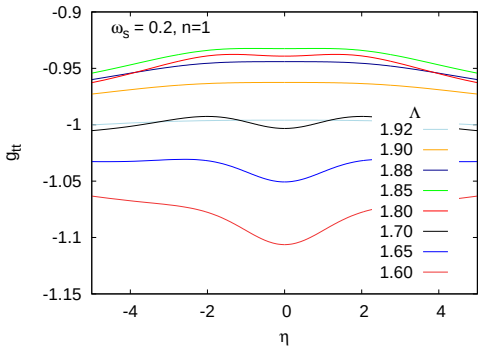
To get further insight into the geometry of these wormholes we exhibit in Fig. 5 also isometric embeddings of the equatorial plane for the same two solutions. We see that for the larger self-coupling parameter the throat is more prolonged. Note that the embedding is euclidean close to the throat, but pseudo-euclidean otherwise.

Let us finally consider the static orbits. As examples we consider rotating wormhole solutions with $\omega_s = 0.2$. In Fig.6 we show the metric component g_{tt} in the equatorial plane as a function of η. Stable static orbits exist only for values of Λ larger than ≈ 1.6. If $\Lambda > 1.85$ a single stable static orbit is located at the throat. For smaller values of Λ two stable static orbits exist, located symmetrically to the left and to the right of the throat, while the static orbit at the throat becomes unstable. For $\Lambda < 1.6$ only the unstable static orbit at the throat remains.

For the sequences of rotating wormhole solutions with $\omega_s > 0.2$, we considered in our study, no stable static orbits were found.

IV. CONCLUSIONS

In this paper we have considered wormhole solutions supported by a complex phantom field with a Mexican hat type potential in Einstein gravity. The complex phantom field allows for an explicit dependence on time and azimuthal



(a)

Figure 6: Static orbits: We show the metric component g_{tt} in the equatorial plane as a function of η for $\omega_s = 0.2$ and several values of Λ.

angle, while still retaining a stationary axially symmetric metric. The $U(1)$ invariance of the model gives rise to a conserved current and an associated conserved charge, the particle number.

Analogous to boson stars and wormholes immersed in ordinary bosonic matter, the harmonic time-dependence includes a boson frequency ω_s, whereas the angular-dependence involves a winding number n, and the angular momentum turns out to be proportional to the particle number with proportionality constant n.

However, the analogy between the known systems based on ordinary complex boson fields and those based on a complex phantom field considered here does not carry much further. In particular, in the presence of the complex phantom field there arise static solutions, i.e., solutions where the boson frequency vanishes, which are non-singular everywhere and asymptotically flat and possess a finite mass.

In the case of rotation, where n assumes a finite value, these solutions with vanishing boson frequency give rise to deformed static wormholes. Here the n-dependence results in an explicit dependence of the phantom field and the metric on the polar angle. For finite boson frequency the rotation of the phantom field drags the throat and the spacetime along, allowing for symmetric rotating wormholes.

For $n = 0$ the wormhole solutions exist for a large range of values of the self-interaction of the phantom field. Indeed, the coupling constant can be made arbitrarily large. In contrast, the $n > 0$ wormholes solutions seem to exist only in a small interval of the coupling constant, which decreases with increasing boson frequency.

As the coupling constant increases for a fixed boson frequency, at a certain point the solutions change rapidly. Their mass decreases steeply, their particle number and angular momentum increase steeply together with the circumferential radius of the throat. At the same time the angular frequency in the equatorial plane tends towards zero. Unfortunately, the accuracy of the solutions then deteriorates, and we cannot draw a reliable conclusion on the limiting behavior.

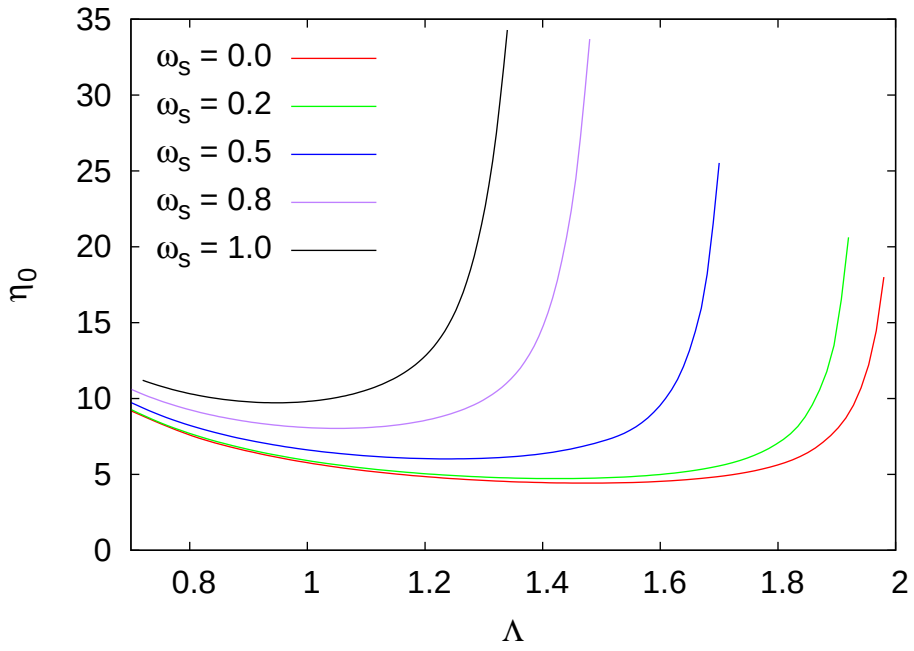
Concerning the stability of these wormhole spacetimes we recall that in the non-rotating case they have been shown to possess an unstable radial mode [45], in complete analogy to the static Ellis wormholes [60–63]. While for rotating wormholes in four spacetime dimensions, such an analysis would be much more involved, one might consider to study the rotating case first in five dimensions, where it has been shown, that the notorius radial instability may disappear [64].

Acknowledgments

We would like to acknowledge support by the DFG Research Training Group 1620 *Models of Gravity* as well as by the COST Action CA16104 *GWverse*. We are grateful to the Research Group Linkage Programme of the Alexander von Humboldt Foundation for the support of this research. XYC would like to thank Lucas G. Collodel and Jose Luis Blázquez-Salcedo for useful discussion.

[1] J. G. Cramer, R. L. Forward, M. S. Morris, M. Visser, G. Benford and G. A. Landis, Phys. Rev. D **51** (1995) 3117.
[2] M. Safonova, D. F. Torres and G. E. Romero, Phys. Rev. D **65** (2002) 023001.
[3] V. Perlick, Phys. Rev. D **69** (2004) 064017.
[4] K. K. Nandi, Y. Z. Zhang and A. V. Zakharov, Phys. Rev. D **74** (2006) 024020.

[5] F. Abe, Astrophys. J. **725**, 787 (2010).
[6] Y. Toki, T. Kitamura, H. Asada and F. Abe, Astrophys. J. **740** (2011) 121.
[7] K. Nakajima and H. Asada, Phys. Rev. D **85** (2012) 107501.
[8] N. Tsukamoto, T. Harada and K. Yajima, Phys. Rev. D **86** (2012) 104062.
[9] P. K. F. Kuhfittig, Eur. Phys. J. C **74** (2014) no.99, 2818.
[10] C. Bambi, Phys. Rev. D **87** (2013) 107501.
[11] R. Takahashi and H. Asada, Astrophys. J. **768** (2013) L16.
[12] N. Tsukamoto and T. Harada, Phys. Rev. D **95** (2017) no.2, 024030.
[13] P. G. Nedkova, V. K. Tinchev and S. S. Yazadjiev, Phys. Rev. D **88** (2013) no.12, 124019.
[14] T. Ohgami and N. Sakai, Phys. Rev. D **91**, 124020 (2015).
[15] R. Shaikh, Phys. Rev. D **98** (2018) no.2, 024044.
[16] G. Gyulchev, P. Nedkova, V. Tinchev and S. Yazadjiev, Eur. Phys. J. C **78** (2018) no.7, 544.
[17] T. Harko, Z. Kovacs and F. S. N. Lobo, Phys. Rev. D **78**, 084005 (2008).
[18] T. Harko, Z. Kovacs and F. S. N. Lobo, Phys. Rev. D **79**, 064001 (2009).
[19] C. Bambi, Phys. Rev. D **87**, 084039 (2013).
[20] M. Zhou, A. Cardenas-Avendano, C. Bambi, B. Kleihaus and J. Kunz, Phys. Rev. D **94**, 024036 (2016).
[21] F. Lamy, E. Gourgoulhon, T. Paumard and F. H. Vincent, Class. Quant. Grav. **35** (2018) no.11, 115009.
[22] T. Damour and S. N. Solodukhin, Phys. Rev. D **76**, 024016 (2007).
[23] M. Azreg-Ainou, JCAP **1507**, 037 (2015).
[24] V. Dzhunushaliev, V. Folomeev, B. Kleihaus and J. Kunz, JCAP **1608**, no. 08, 030 (2016).
[25] V. Cardoso, E. Franzin and P. Pani, Phys. Rev. Lett. **116**, 171101 (2016) Erratum: [Phys. Rev. Lett. **117**, 089902 (2016)].
[26] R. A. Konoplya and A. Zhidenko, JCAP **1612**, 043 (2016).
[27] K. K. Nandi, R. N. Izmailov, A. A. Yanbekov and A. A. Shayakhmetov, Phys. Rev. D **95**, 104011 (2017).
[28] P. Bueno, P. A. Cano, F. Goelen, T. Hertog and B. Vercnocke, Phys. Rev. D **97**, 024040 (2018).
[29] J. L. Blázquez-Salcedo, X. Y. Chew and J. Kunz, Phys. Rev. D **98** (2018) no.4, 044035.
[30] M. S. Morris, K. S. Thorne, Am. J. Phys. **56**, 395 (1988).
[31] M. S. Morris, K. S. Thorne and U. Yurtsever, Phys. Rev. Lett. **61**, 1446 (1988).
[32] H. G. Ellis, J. Math. Phys. **14**, 104 (1973).
[33] K. A. Bronnikov, Acta Phys. Polon. **B4**, 251 (1973).
[34] T. Kodama, Phys. Rev. **D18**, 3529 (1978).
[35] H. G. Ellis, Gen. Rel. Grav. **10**, 105 (1979).
[36] F. S. N. Lobo, Phys. Rev. D **71**, 084011 (2005).
[37] F. S. N. Lobo, Fundam. Theor. Phys. **189**, pp. (2017).
[38] P. E. Kashargin and S. V. Sushkov, Grav. Cosmol. **14**, 80 (2008).
[39] P. E. Kashargin and S. V. Sushkov, Phys. Rev. D **78**, 064071 (2008).
[40] B. Kleihaus and J. Kunz, Phys. Rev. D **90**, 121503 (2014).
[41] X. Y. Chew, B. Kleihaus and J. Kunz, Phys. Rev. D **94**, 104031 (2016).
[42] B. Kleihaus and J. Kunz, Fundam. Theor. Phys. **189**, 35 (2017).
[43] X. Y. Chew, B. Kleihaus and J. Kunz, Phys. Rev. D **97** (2018) no.6, 064026.
[44] C. Hoffmann, T. Ioannidou, S. Kahlen, B. Kleihaus and J. Kunz, Phys. Lett. B **778**, 161 (2018).
[45] V. Dzhunushaliev, V. Folomeev, B. Kleihaus and J. Kunz, Phys. Rev. D **97** (2018) no.2, 024002.
[46] P. Jetzer, Phys. Rept. **220**, 163 (1992).
[47] T. D. Lee, Y. Pang, Phys. Rept. **221**, 251 (1992).
[48] F. E. Schunck, E. W. Mielke, Class. Quant. Grav. **20**, R301 (2003).
[49] S. L. Liebling and C. Palenzuela, Living Rev. Rel. **15**, 6 (2012).
[50] F. E. Schunck and E. W. Mielke, in *Relativity and Scientific Computing: Computer Algebra, Numerics, Visualization*, eds. F. W. Hehl, R. A. Puntigam, and H. Ruder, (Springer Berlin Heidelberg, 1996).
[51] F. E. Schunck and E. W. Mielke, Phys. Lett. A **249**, 389 (1998).
[52] F. D. Ryan, Phys. Rev. D **55**, 6081 (1997).
[53] S. Yoshida and Y. Eriguchi, Phys. Rev. D **56**, 762 (1997).
[54] F. E. Schunck and E. W. Mielke, Gen. Rel. Grav. **31**, 787 (1999).
[55] B. Kleihaus, J. Kunz and M. List, Phys. Rev. D **72**, 064002 (2005).
[56] B. Kleihaus, J. Kunz, M. List and I. Schaffer, Phys. Rev. D **77**, 064025 (2008).
[57] C. Hoffmann, T. Ioannidou, S. Kahlen, B. Kleihaus and J. Kunz, Phys. Rev. D **97**, 124019 (2018).
[58] L. G. Collodel, B. Kleihaus and J. Kunz, Phys. Rev. Lett. **120** (2018) no.20, 201103.
[59] W. Schönauer and R. Weiß, J. Comput. Appl. Math. 27, 279 (1989) 279;
M. Schauder, R. Weiß and W. Schönauer, *The CADSOL Program Package*, Universität Karlsruhe, Interner Bericht Nr. 46/92 (1992).
[60] H. -a. Shinkai and S. A. Hayward, Phys. Rev. D **66**, 044005 (2002).
[61] J. A. Gonzalez, F. S. Guzman, and O. Sarbach, Class. Quant. Grav. **26**, 015011 (2009).
[62] J. A. Gonzalez, F. S. Guzman, and O. Sarbach, Class. Quant. Grav. **26**, 015010 (2009).
[63] T. Torii and H. a. Shinkai, Phys. Rev. D **88**, 064027 (2013).
[64] V. Dzhunushaliev, V. Folomeev, B. Kleihaus, J. Kunz and E. Radu, Phys. Rev. D **88**, 124028 (2013).


35
30
25
20
15
10
5
0
0.8
1
1.2
1.4
1.6
1.8
2
η_0
Λ
ω_s = 0.0
ω_s = 0.2
ω_s = 0.5
ω_s = 0.8
ω_s = 1.0